



Single-Layer Graphene Enhances the Osteogenic Differentiation of Human Mesenchymal Stem Cells *In Vitro* and *In Vivo*

Yunsong Liu^{1,†}, Tong Chen^{1,†}, Feng Du^{2,3}, Ming Gu¹, Ping Zhang¹, Xiao Zhang¹, Jianzhang Liu¹, Longwei Lv¹, Chunyang Xiong^{2,3,*}, and Yongsheng Zhou^{1,4,*}

¹Department of Prosthodontics, Peking University School and Hospital of Stomatology, Beijing 100081, China

²Department of Mechanics and Engineering Science, College of Engineering, Peking University, Beijing 100871, China

³Academy for Advanced Interdisciplinary Studies, Peking University, Beijing 100871, China

⁴National Engineering Laboratory for Digital and Material Technology of Stomatology, Beijing 100081, China

In recent years, although several studies have demonstrated the potential of graphene-coated substrates in promoting attachment, proliferation and differentiation of osteoblasts and mesenchymal stem cells (MSCs), the effects of single-layer graphene on the osteogenic differentiation of human MSCs (hMSCs) remains unclear, especially *in vivo*. In this study, we transferred chemical vapor deposition (CVD) grown single-layer graphene to glass slides and observed its effects on adhesion, proliferation and osteogenic differentiation of human adipose-derived stem cells (hASCs) and human bone marrow mesenchymal stem cells (hBMMSCs) *in vitro*. Then, *in vivo*, we incubated hASCs and hBMMSCs on single-layer graphene-coated smooth titanium (Ti) disks before implanting them into the back subcutaneous area of nude mice. We found that single-layer graphene accelerated cell adhesion to the substrate without influencing cell proliferation of hMSCs. Moreover, we present the first study that explores the epigenetic role of single-layer graphene in determining stem cell fate. By utilizing epigenetic approaches, we reveal that single-layer graphene promotes osteogenic differentiation of hMSCs both *in vitro* and *in vivo*, potentially by upregulating methylation of H3K4 at the promoter regions of osteogenesis-associated genes. Overall, our results highlight the potential of this material in implants and injured tissues in clinical applications.

KEYWORDS: Graphene, Mesenchymal Stem Cells, Osteogenic Differentiation, Epigenetics.

INTRODUCTION

Bone tissue engineering, a procedure aimed at regenerating new functional bone, has recently emerged as a promising method for treating bone defects. The technique requires a scaffold that enables cell attachment and maintenance of cell function, along with a rich source of seed cells combined with selected osteoinductive growth factors.¹ Mesenchymal stem cells (MSCs), such as human bone marrow mesenchymal stem cells (hBMMSCs) and human adipose-derived stem cells (hASCs), have the potential to differentiate into osteoblasts, adipocytes and

chondrocytes.² In the past, multiple growth factors and inducers have been administered to promote their differentiation. However, most are difficult and expensive to produce and there are important issues with regards to their safety and the control of their spatiotemporal release.^{3,4} Therefore, there is an increasing need to pursue active osteoinductive or pro-osteogenic differentiation properties that confer stable and long lasting promotion or inductive effects on scaffold materials *in vivo*.

Graphene, a one-atom-thick sheet of carbon atoms arranged in a 2D honeycomb structure, was first isolated by Novoselov and Geim in 2004.⁵ Since then, it has attracted much interest from various fields and become extensively studied by material scientists, physicists and chemists.^{6–11} Now its uses are expanding beyond electronic and chemical applications toward biomedical areas, such

*Authors to whom correspondence should be addressed.

Emails: cyxiong@pku.edu.cn, kqzhouysh@hsc.pku.edu.cn

†These two authors contributed equally to this work.

Received: 6 July 2015

Revised/Accepted: 10 December 2015

as drug delivery, cancer therapies, biosensing and tissue engineering.^{12,13}

Single-layer graphene can now be successfully produced in large areas by chemical vapor deposition (CVD) on copper foil or nickel film;^{14,15} the copper or nickel is etched before the single-layer graphene is transferred to different substrates.¹⁶ Several studies have reported encouraging results with regards the adhesion, proliferation and osteogenic differentiation of MSCs on multiple-layer graphene, graphene oxide (GO) and other graphene hybrid materials.^{17–21} We think it probable that single-layer graphene, which can be synthesized in a relatively pure form, is capable of representing all such materials for investigatory purposes, including *in vivo*.^{14,15}

However, the mechanism by which single-layer graphene increases osteogenic differentiation of MSCs has not been fully revealed.²²

In this study, we transferred CVD grown single-layer graphene to a glass slide and observed its effects on the adhesion, proliferation and differentiation of hASCs and hBMMSCs *in vitro*. Then, *in vivo*, we incubated hASCs and hBMMSCs on single-layer graphene-coated smooth titanium (Ti) disks, and evaluated ectopic bone formation on the Ti disks using nude mice. Furthermore, we utilized epigenetic approaches to explore how graphene directs the osteogenic differentiation of MSCs.

MATERIALS AND METHODS

Ethics Statement

This study was approved by the Ethics Committee of the Peking University Health Science Center, Beijing, China (PKUSSIRB-2013023). All animal experiments were performed in accordance with the approved animal protocol of the Peking University Health Science Center. All surgery was performed under sodium pentobarbital anesthesia. Any potential for suffering was minimized.

Preparation of Graphene Sheets on Glass Slides and Smooth Ti Disks

We purchased CVD grown single-layer graphene on a copper foil substrate from the American Chemical Society (ACS), and cut into opportune sizes. PMMA (950 K grade, 2 wt% in chlorobenzene) was spin-coated on the surface of graphene via a two-step process (step 1: 600 rpm for 10 seconds; step 2: 3000 rpm for 40 seconds) using a Laurell® WS-400BZ-6NPP/LITE spin coater. Next, we cured the deposited PMMA at 180 °C for 4 min. The copper foil substrate was then etched using iron(III) chloride solution (0.05 g/mL in water), and the PMMA (top)/graphene (bottom) film floated to the surface of the solution. After rinsing the film with distilled water twice, a glass slide or Ti disk was placed in de-ionized water with a tilting angle of 30° underneath the floating film. The glass slides or smooth Ti disks (99.6% purity, Leiden, Beijing,

China) were carefully raised from the water to make contact with the graphene. Finally, the top layer of PMMA was removed by bathing in acetone for 30 min. Before the transfer, glass slides or Ti disks were cleaned in acetone for 30 minutes and de-ionized water three times using an ultrasonic cleaning machine. Single-layer graphene-coated glass slides were used for *in vitro* experiments because glass slides are transparent and convenient for the observation of staining results; single-layer graphene-coated Ti disks were used for *in vivo* implantation.

Culture and Osteogenic Induction of hASCs and hBMMSCs

All materials were purchased from Sigma-Aldrich (St. Louis, MO, USA) unless otherwise stated. Human ASCs and hBMMSCs were purchased from Sciencell Research Laboratories (San Diego, CA, USA). Dulbecco's modified Eagle's medium (DMEM), fetal bovine serum (FBS), 100× penicillin and streptomycin mixture were purchased from Gibco (Grand Island, NY, USA). Human ASCs and hBMMSCs were cultured in proliferation medium (PM), which comprised fresh DMEM containing 10% (v/v) FBS, 100 U/mL penicillin G and 100 mg/mL streptomycin, at 37 °C in an incubator with an atmosphere consisting of 95% air, 5% CO₂ and 100% relative humidity. For *in vitro* experiments, we used cells at the fourth passage; all experiments were repeated three times using hMSCs from the three donors, respectively. Osteogenic inducing medium (osteogenic medium, OM) comprised fresh DMEM containing 10% (v/v) FBS, 100 U/mL penicillin G and 100 mg/mL streptomycin, 10 nM dexamethasone, 10 mM β-glycerophosphate and 50 μg/mL L-ascorbic acid.

Adhesion and Proliferation Assay

We counted the number of cells adhered to the surfaces using cell counting kit-8 (CCK8; Dojindo Laboratories, Kumamoto, Japan). Human ASCs and hBMMSCs were seeded at 1.0×10^4 cells per well on glass slides coated with single-layer graphene and glass slides without graphene, respectively, in a 24-well plate. After 2, 12 and 24 h of cell culture. The protocol used accorded with the manufacturer's instructions and with that used by us previously.²³

We prepared samples for scanning electron microscopy (SEM) according to the method reported by us previously and viewed them using a field emission SEM (FESEM, Hitachi, S4800, Japan).²⁴ Again, according to methods reported by us previously, we examined samples using a Confocal Zeiss Axiovert 650 microscope (Carl Zeiss Microimaging, LLC, Thornwood, NY, USA) at 488 nm (green) and 405 nm (blue) wavelengths.^{23,24} Human ASCs and hBMMSCs proliferation was also measured using CCK8 after 0, 2, 4, 6 and 8 days of cell culture on different surfaces.

Alkaline Phosphatase (ALP) Staining of hASCs and hBMMSCs on Graphene

For ALP staining, hASCs and hBMMSCs were seeded on glass slides coated with single-layer graphene at the same density as above in 24-well plates; a glass slide without graphene was used as the control surface. The experiment was performed using an ALP staining kit according to the manufacturer's protocol, as previously described.²⁵

Alizarin Red S (AR-S) Staining and Mineralization Assays

Human ASCs and hBMMSCs were seeded as above in 24-well plates. Mineralization was evaluated using an AR-S staining kit, according to the manufacturer's protocol, and as previously described by us.^{25,26}

RNA Extraction, Reverse Transcription and Quantitative Real-Time PCR

Human ASCs and hBMMSCs were seeded as above in 6-well plates. Total cellular RNAs were isolated on 7 and 14 days after osteoinduction using the Trizol reagent (Invitrogen, Carlsbad, CA, USA) and used to synthesize first strand cDNA using the reverse transcription system (Roche, Basel, Switzerland). Quantification of all gene transcripts was performed by real-time polymerase chain reaction (qPCR) using a Power SYBR Green PCR Master Mix and an ABI PRISM 7500 sequence detection system (Applied Biosystems, Foster City, CA, USA). β -actin expression was detected as the internal control. The primers used are shown in Table I. The cycle threshold values (Ct values) were used to calculate the fold differences by the $\Delta\Delta$ Ct method.²⁷

Immunofluorescence

Samples were prepared for immunofluorescence according to the method described by us previously.^{24,25} To detect vinculin, 1:200 anti-vinculin primary antibody (Santa Cruz, Dallas, TX, USA) was used; to detect osteocalcin, 1:200 anti-osteocalcin primary antibody (Santa Cruz, Dallas, TX, USA) was used. The procedures used for the incubation of the secondary antibody and 6-diamidino-2-phenylindole (DAPI) were as described previously.^{23,24} Samples were examined using a Confocal Zeiss Axiovert 650 microscope (Carl Zeiss Microimaging, Oberkochen, Germany) using 488 nm (green, osteocalcin),

543 nm (red, vinculin) and 405 nm (blue, DAPI) wavelengths, respectively. For quantification of vinculin expression, 10 images of each sample were taken randomly, and the number of vinculin positive tips of cell pseudopodium were counted and subjected to statistical analysis. To examine the methylation of H3K4, 1:500 anti-tri-H3K4-methylation primary antibody (Cell Signaling Technology) was used.

Ectopic Bone Formation *In Vivo*

Human ASCs and hBMMSCs were incubated on Ti disks coated with single-layer graphene. The disks were then implanted into the back subcutaneous area of nude mice for our *in vivo* study, referring to Hall et al.'s study design.²⁸ Human ASCs and hBMMSCs-coated Ti disks without graphene were used as controls, while Ti disks without cells and graphene were used as blank controls. Implants were divided into five groups: disks without cells (no cells), disks coated with hASCs cultured in proliferation medium (hASCs without OI), disks coated with hASCs cultured in osteoinducing medium (hASCs with OI), disks coated with hBMMSCs cultured in proliferation medium (hBMMSCs without OI) and disks coated with hBMMSCs cultured in osteoinducing medium (hBMMSCs with OI). In each group, disks with single-layer graphene and disks without graphene were included to investigate the effect of graphene on bone formation *in vivo*. Seven days after *in vitro* culture, eight-week-old male BalB/c nude mice were anaesthetized with pentobarbital, and the above implants were placed aseptically into the dorsal subcutaneous area. At four and eight weeks after surgery, implants were harvested together with their surrounding tissues (10 implants for each group). Tissues were fixed by formalin, infiltrated by resin and hard tissue slices were observed under light microscope after HE and toluidine blue staining.

For the soft X-ray examination, 2 mm thick hard tissue slice was prepared for each sample. Then, the slices were radiographed with digital radiographic apparatus (GE Senograph 2000D, USA) under condition of 25 KV, 50 mAs, and 50 cm distance. Gray scales of the regions of interest (ROI) were then analyzed with medical image analyzing software (ImageJ 1.44p, NIH, USA). The gray scale of 2 mm thick vertebral body slice was detected as positive control and the relative gray scales of different groups were compared as previously described.²⁶

Table I. Sequences of primers used for real-time PCR.

Gene	Forward primer	Reverse primer
Runx2	ATGGGATGGGTGTCTCCACA	CCACGAAGGGGAACCTTGTC
OSX	CCTCCTCAGCTCACCTTCTC	GTTGGGAGCCCAATAGAAA
OCN	CACTCCTCGCCCTATTGGC	CCCTCCTGCTTGACACAAAG
RBP2	GTCCAGCGCCTGAAT- GAACTT	GCAACAATCTTGCTCAAA- GCATA
β -actin	CATGTACGTTGCTATCCAGGC	CTCCTTAATGTCACGCACGAT

Chromatin Immunoprecipitation Assay (ChIP Assay) and Real-Time PCR

Human ASCs and hBMMSCs were crosslinked in 1% formaldehyde at 37 °C for 10 min and resuspended in 200 μ L lysis buffer (1% SDS, 10 mM EDTA and 50 mM Tris-HCl) and nuclear lysates were sonicated and diluted 10-fold with immunoprecipitation buffer (16.7 mM Tris-HCl, pH 8.1; 167 mM NaCl; 1.2 mM EDTA; 0.01%

SDS; and 1.1% TritonX-100). Lysates were then immunoprecipitated with non-specific rabbit IgG, H3K4me3, H3K4me2, H3K4me1 (all from Cell Signaling Technology, Cambridge, MA) for 12 h at 4 °C. Immune complexes were incubated with Protein G-Sepharose CL-4B (GE Healthcare, Piscataway, NJ) for 2 h at 4 °C. After successive washings, immune complexes containing DNA were purified and eluted, and the precipitated DNA was amplified by PCR. Primer pairs used in this study were as follows: OCN promoter, (forward) 5'-GTGGCTCACCTCCATCAC-3' and (reverse) 5'-CCTCCAGCACTGTTTATACCCT-3' and Runx2 promoter, (forward) 5'-GGCTCCTTCAGCATTTGTATTC-3' and (reverse) 5'-GCTCTTTCTCTCTCTCTTTCTC-3'.

Statistics Analysis

Data are expressed as the mean \pm standard deviation and analyzed using SPSS software (SPSS Inc., Chicago, IL, USA). Student's *t*-test was performed. For all tests, statistical significance was accepted at *p*-values lower than 0.05.

RESULTS

Surface Characterization

Atomic force microscope (AFM) observation (Fig. 1(A)) demonstrated a significant increase in surface roughness (measured by the root mean square (RMS) of the profile) of the glass slide coated with single-layer graphene compared with the glass slide without any graphene coating ($p < 0.05$), while no significant differences were observed between Ti disk coated with single-layer graphene and Ti disk without graphene ($p > 0.05$). The Raman spectra revealed a typical fingerprint of single-layered graphene: a very sharp and symmetric 2D band at around 2680 cm^{-1} , and a relatively weaker peak of G band at around 1580 cm^{-1} (Fig. 1(B)). The water contact angle showed that the wettability of the glass slide increased significantly ($p < 0.05$) when coated with single-layer graphene compared with no graphene coating. However, no significant differences ($p > 0.05$) were observed between Ti disk coated with single-layer graphene and Ti disk without graphene (Fig. 1(C)).

Adhesion and Proliferation of hASCs and hBMMSCs on Graphene

Using SEM (Fig. 2(A)), we observed morphology and fine structures of the adhered cells, while, using confocal microscopy photographs of FITC-phalloidin staining (Fig. 2(B)), we observed morphology of the adhered cells. After 12 h of culture, we observed extended lamellipodia for the cells coated with a single-layer of graphene on the glass slide (graphene group), while we observed a relatively short pseudopodium extension for the graphene-absent group. Using CCK8, our cell counting assay for

hASCs and hBMMSCs demonstrated that at 2, 12 and 24 h after culture, cells were more adherent ($p < 0.05$) in the graphene group compared with the graphene-absent group (Fig. 2(C)). For cell proliferation, we observed a logarithmic proliferation curve for hASCs and hBMMSCs for both groups (graphene group and graphene-absent), with no significant differences observed between the two groups over two to eight days (Fig. 2(D)).

To investigate the mechanism by which hMSCs adhered faster to the surface of graphene at the early stage of culture, we applied immunofluorescence staining to determine vinculin protein expression levels. As shown in Figures 2(E and F), we observed more vinculin positive tips of cell pseudopodium in the graphene group compared with the graphene-absent group after 12 and 24 h of culture ($p < 0.05$).

Osteogenic Differentiation of hASCs and hBMMSCs on Graphene

After 14 days of culture with or without osteoinduction (OI), alkaline phosphatase (ALP) staining showed that the graphene group exhibited greater positive staining compared with the graphene-absent group for both hASCs and hBMMSCs (Fig. 3(A)). AR-S staining and mineralization assays demonstrated that after 21 days of culture with or without OI, the AR-S stained specimens revealed that the graphene group exhibited increased red staining compared with the graphene-absent group for both hASCs and hBMMSCs (Fig. 3(B)). Mineralization assays for both hASCs and hBMMSCs (Fig. 3(C)) demonstrated that the graphene group was more mineralized compared with the graphene-absent group after 21 days of culture with or without OI ($p < 0.05$).

Osteocalcin (OCN) protein expression detected by immunofluorescence showed that after 14 days of OI, hASCs and hBMMSCs cultured on the graphene surface had stronger OCN-positive staining compared with the graphene-absent group (Fig. 3(D)).

We investigated gene expression of osteogenic-related genes Runx2, Osterix (OSX) and OCN (Fig. 3(E)). After seven days of OI, the relative expression of Runx2 and OCN in hASCs on the graphene surface was higher compared with the graphene-absent group ($p < 0.05$), while relative expression levels of Runx2, OSX and OCN in hBMMSCs on the graphene surface was higher compared with the graphene-absent group ($p < 0.05$). After 14 days of OI, expression levels of Runx2, OSX and OCN in hASCs and hBMMSCs were higher in the graphene group compared with the graphene-absent group ($p < 0.05$). Interestingly, even when cultured without OI, relative Runx2 and OCN expression in hASCs and hBMMSCs was higher in the graphene group compared with the graphene-absent group ($p < 0.05$).

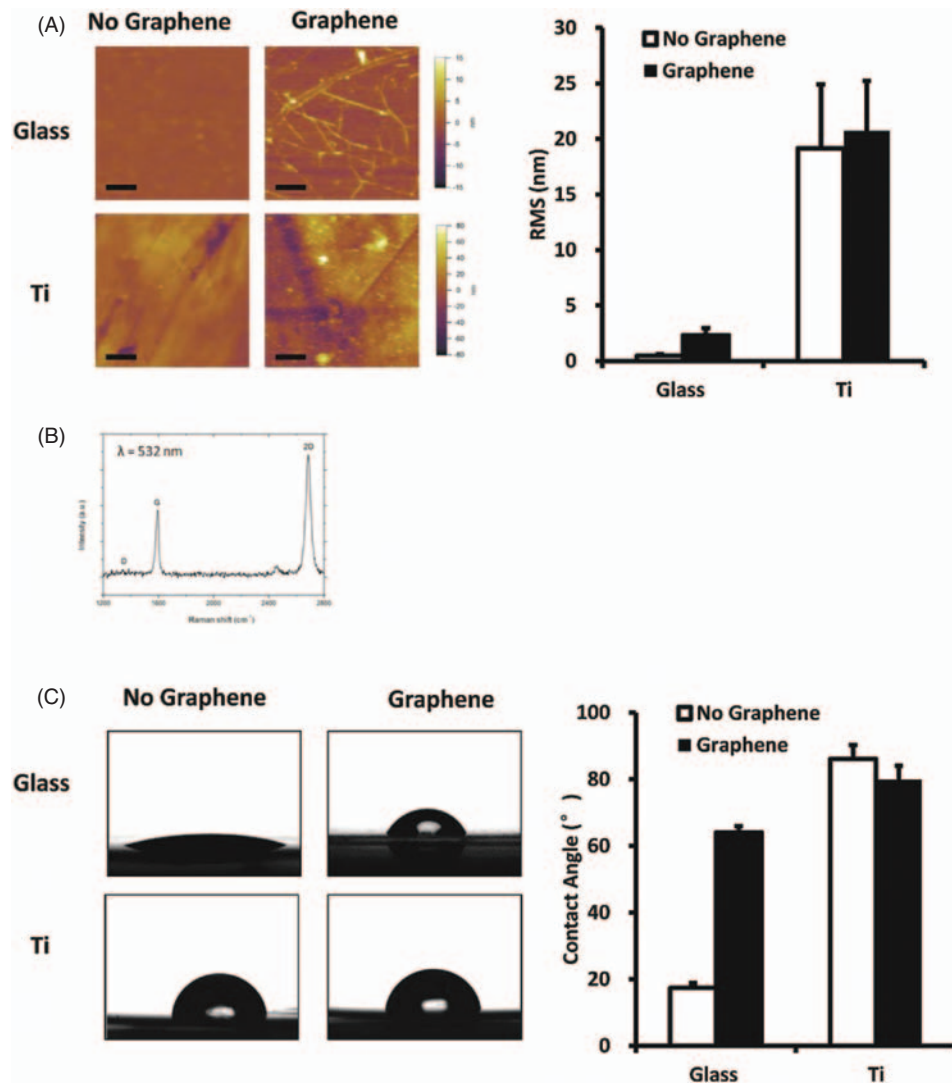


Figure 1. Surface characterization of graphene. (A) Atomic force microscopy (AFM) observation and roughness analysis of graphene and control surfaces. (B) Raman spectroscopy analysis of the graphene surface. (C) Photographs of contact angle measurement of water. * $p < 0.05$.

Ectopic Bone Formation *In Vivo*

After four weeks of implantation, we observed hard tissue slices using light microscopy after HE and toluidine blue staining. HE staining revealed the bone matrix as a uniform acidophilic tissue, while the toluidine blue staining was evenly dark blue with sporadic osteogenic-related cells. We only considered tissue samples that positively stained against both HE and toluidine blue as actual bone formation. Implant surfaces coated with hASCs and hBMMSCs after seven days of OI demonstrated obvious bone matrix formation. Moreover, cells on Ti disks coated with single-layer graphene exhibited larger bone matrix formation (white arrows) compared with cells on Ti disks (graphene-absent). Implant surfaces coated with hASCs and hBMMSCs without OI demonstrated a similar tendency compared with samples with OI. We observed no

typical bone matrix formation on implant surfaces without cells (Fig. 4(A)).

After eight weeks of implantation, ectopic bone formation became more apparent (compared with at four weeks). Moreover, we observed more significant bone matrix formation on the surface of the graphene-coated group compared graphene-absent group. The neo-bone layer reached a thickness of about $30 \mu\text{m}$ (white arrow) in the graphene group with OI for hASCs and hBMMSCs (Fig. 4(B)).

Soft X-ray analyses of ectopic bone formation exhibited a similar tendency with histological results. We observed increased amounts of high density spots in the graphene-coated group compared with the graphene-absent group, especially for the hASCs and hBMMSCs osteoinduction (OI) group (Fig. 4(C)). The relative gray scale percentages of the ectopic bone formation in each group to the positive

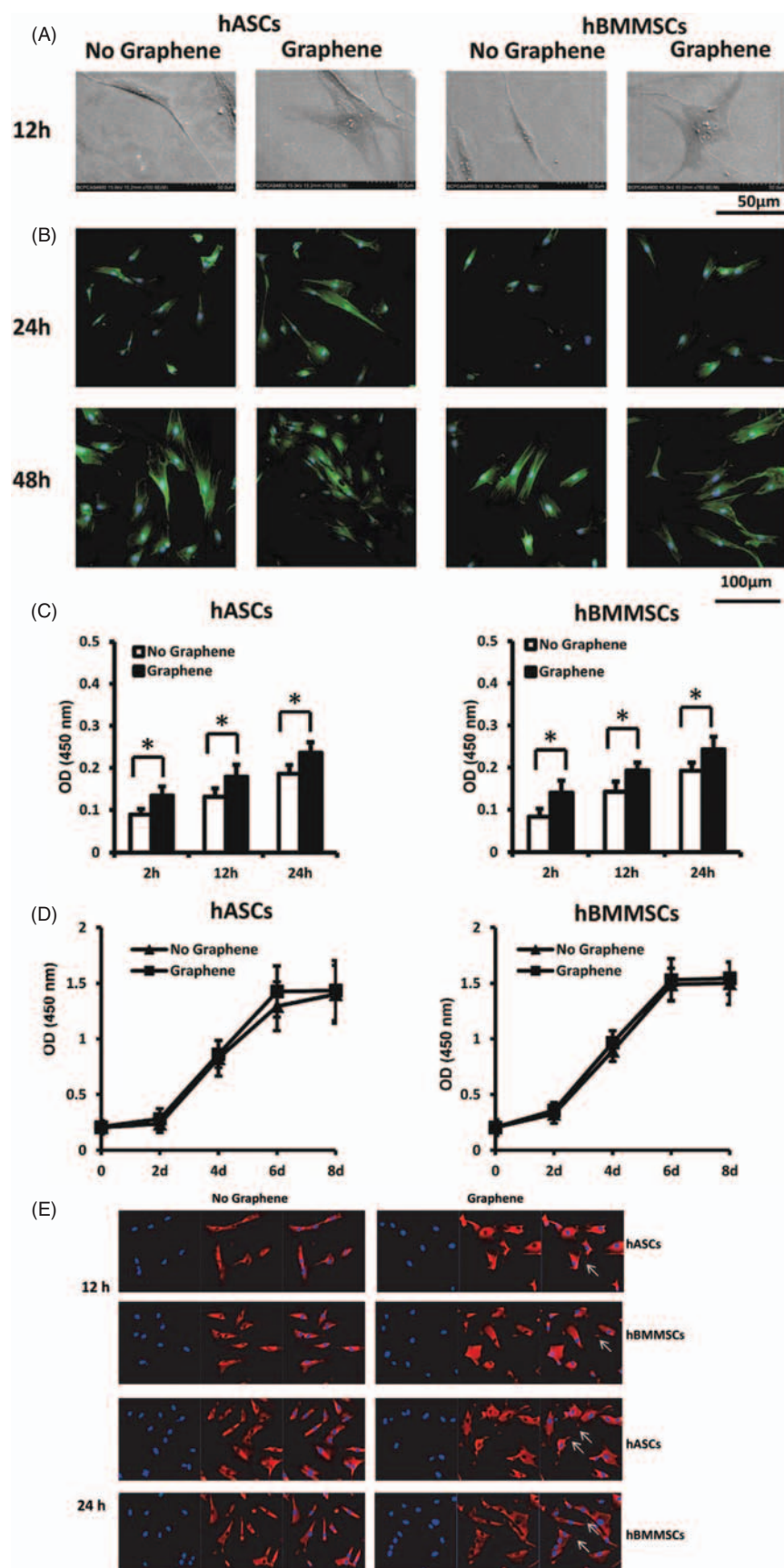


Figure 2. Continued.

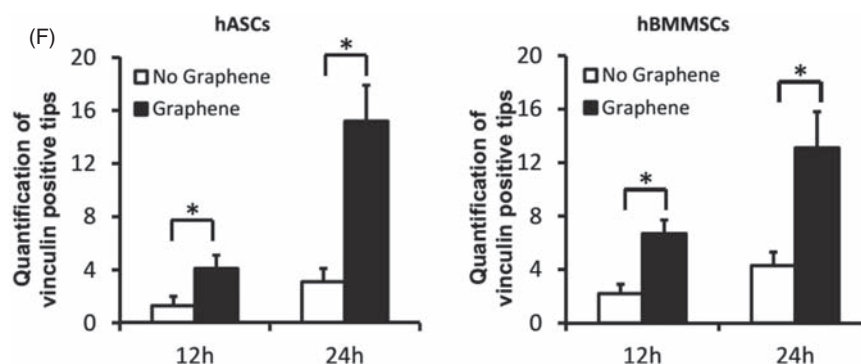


Figure 2. The adhesion and proliferation of human adipose-derived stem cells (hASCs) and human bone marrow derived mesenchymal stem cells (hBMMSCs) on graphene. (A) Scanning electron microscopic observation of hASCs and hBMMSCs on graphene and control surfaces after 12 h of culture at 700 \times magnification. (B) Confocal micrographs of hASCs and hBMMSCs on graphene and control surfaces after 24 h and 48 h of culture at 100 \times magnification. Phalloidin is colored green and nuclei are colored blue. (C) CCK8 assay showing adhering of hASCs and hBMMSCs on graphene and control surfaces after 2 h, 12 h and 24 h of culture. (D) Growth curves of hASCs and hBMMSCs on graphene and control surfaces during eight days of culture. (E) Immunofluorescent staining for vinculin shows stronger vinculin expression at the end of cell pseudopodium (white arrow) in the graphene-coated group compared with the graphene-absent group. (F) Quantification of vinculin positive tips of cell pseudopodium. * $p < 0.05$.

control which reflected osteogenic efficiency were shown in Figure 4(D). The relative gray scale percentages of all graphene-coated groups were significantly higher than the graphene-absent groups ($p < 0.05$).

Epigenetic Regulation of Graphene on hASCs and hBMMSCs

Examination of the tri-methylation level of H3K4 of hASCs and hBMMSCs by immunofluorescence showed that after seven days of OI, the graphene group demonstrated stronger green fluorescence compared with the graphene-absent group. The immunofluorescence of specimens without OI demonstrated a similar, but weaker, tendency compared with samples with OI (Fig. 5(A)). ChIP assays for hASCs and hBMMSCs demonstrated that the tri-methylation of H3K4 at the promoter area of osteogenic genes, including Runx2 and OCN, was significantly enhanced on the surface of graphene compared with graphene-absent group after seven days of culture in osteogenic medium (Fig. 5(B)). After seven days of OI, the relative RBP2 expression in the graphene group with OI was significantly lower ($p < 0.05$) than the graphene-absent group (Fig. 5(D)).

DISCUSSION

The Effects of Single-Layer Graphene on the Adhesion and Proliferation of hASCs and hBMMSCs

Our study demonstrated that at early stages of cell loading, single-layer graphene accelerated cell adhesion to the substrate surface. Our vinculin immunofluorescence staining revealed that the graphene group exhibited stronger vinculin expression at the end of cell pseudopodium

compared with the graphene-absent group. Vinculin is a structural protein associated with focal adhesions (FAs). Our results suggest that the graphene surface may provide an environment for higher affinity of hMSCs on the substrates. Kalbacova et al. previously investigated FAs of cells cultured on the surface of graphene and found that FAs in contact with graphene films are concentrated to the protruding ends of the cells, which was conformable to our results.¹⁷

Numerous material characteristics influence cell adhesion, such as surface roughness, wettability and its mechanical properties.²⁹ Our contact angle measurements showed an increase in the contact angle of the glass slide coated with a single-layer of graphene, and therefore a decrease in wettability. As reported previously, a hydrophilic surface is expected to influence cell assembly and favor cell attachment.³⁰ However, through this study, the quick adhesion of hMSCs on graphene may not be due to the wettability of the surface, but due to the unique properties of graphene. For hMSCs proliferation, although single-layer graphene could accelerate cell adhesion at the early stage of cell loading, there was no significant difference for the rate of cell proliferation between the graphene group and graphene-absent group between two to eight days. Some previous studies have discussed the effect of graphene on cell proliferation; however, their observation times have been relatively limited, their results contradictory and no proliferation curve provided.^{17–19} Our results show that single-layer graphene has no negative effects on the proliferation of hASCs and hBMMSCs, which suggests that the incorporation of this material in implants or injured tissues would not affect the physiological conditions for cells to proliferate.

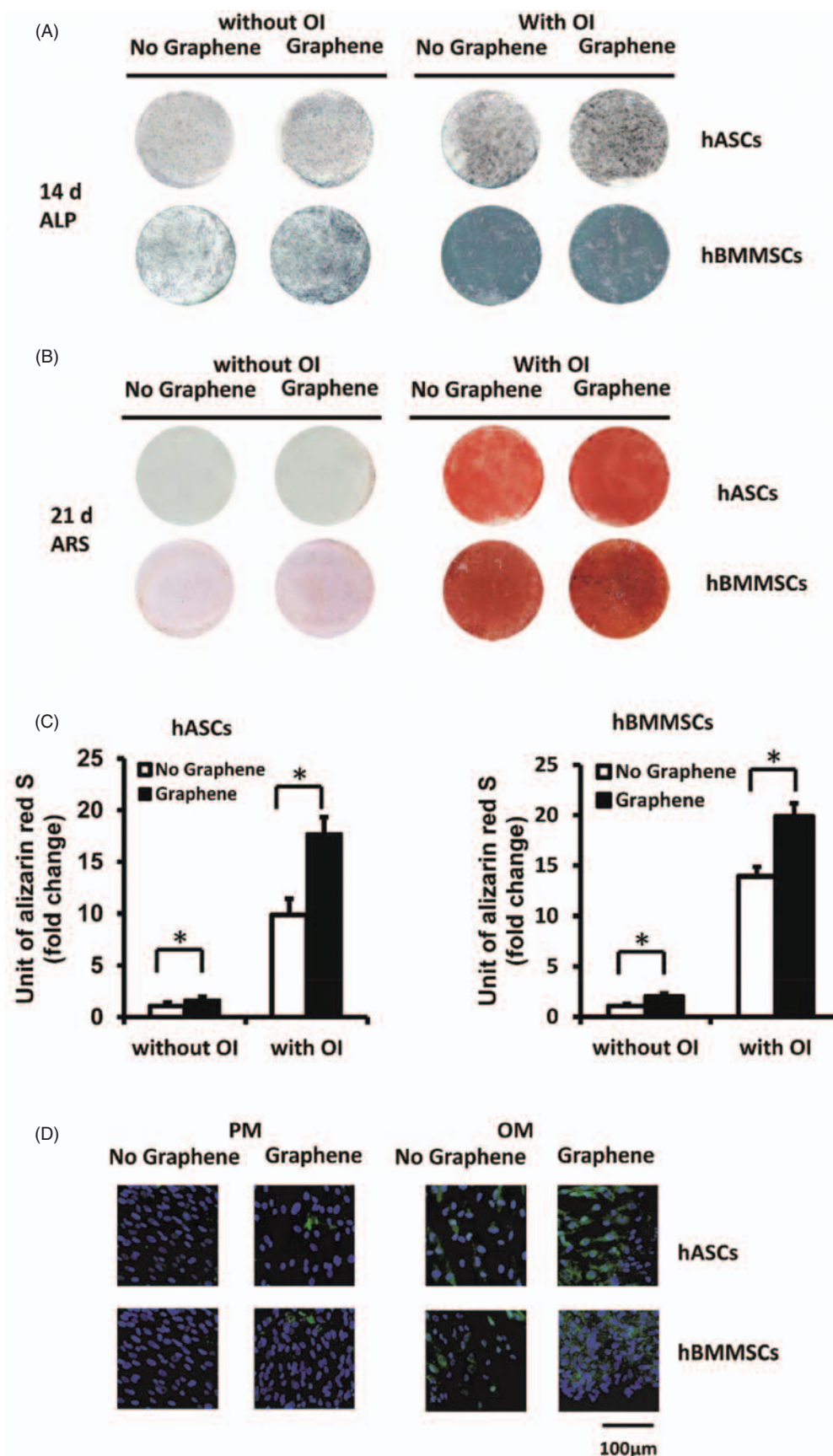


Figure 3. Continued.

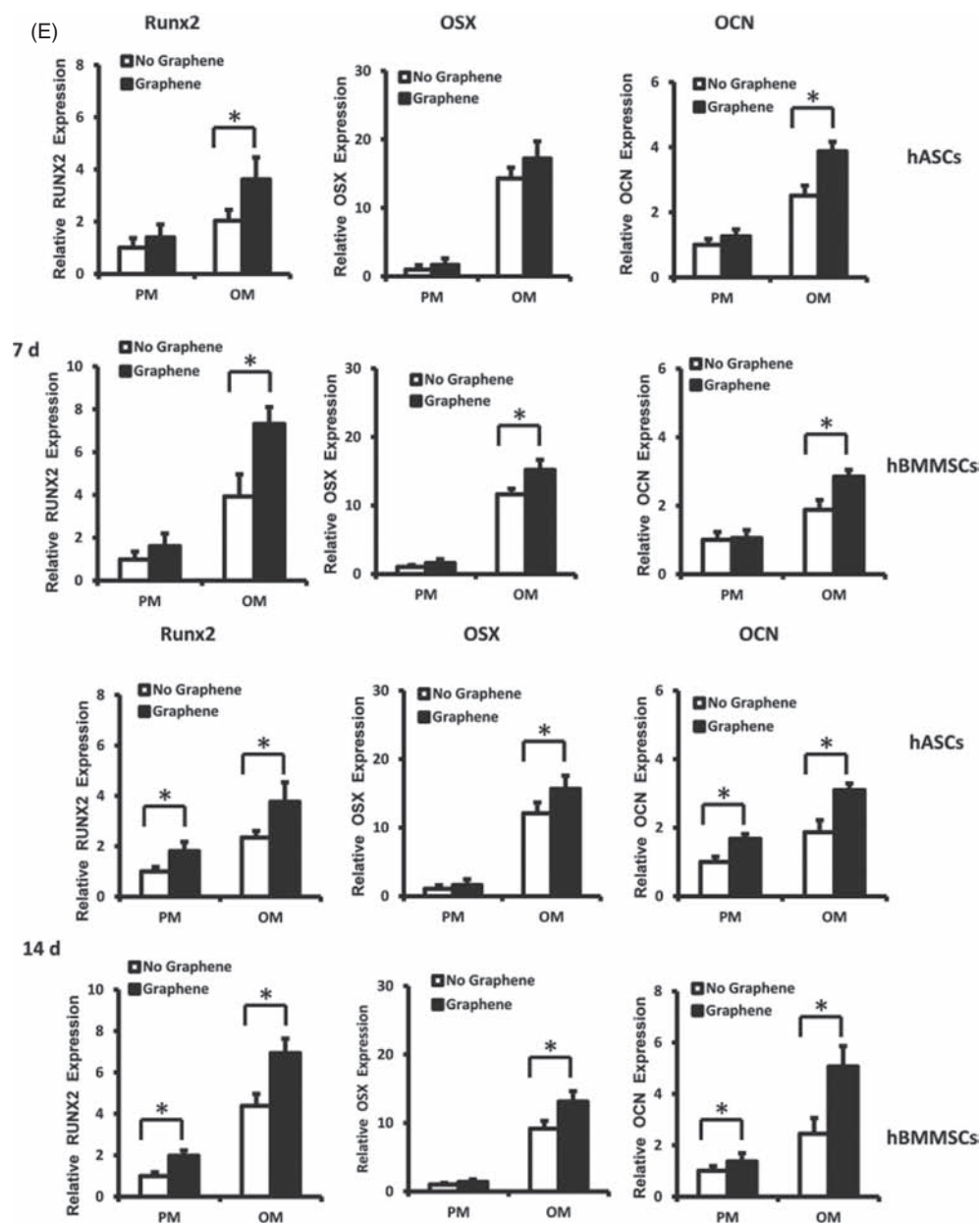


Figure 3. Osteogenic differentiation of hASCs and hBMMSCs on TiO_2 nanotubes *in vitro*. (A) ALP staining of hASCs and hBMMSCs cultured on graphene and control surfaces for 14 days. (B) Alizarin Red staining at 21 days. (C) Mineralization assay at 21 days. (D) Immunofluorescent staining for OCN in hASCs and hBMMSCs cultured on graphene and control surfaces for 14 days at 100 \times magnification. OCN is colored green and nuclei are colored blue. (E) The expression of osteogenic genes in hASCs and hBMMSCs cultured on graphene and control surfaces for seven and 14 days. * $p < 0.05$. PM: proliferation medium; OM: osteogenic medium.

The Effects of Graphene on the Osteogenic Differentiation of hASCs and hBMMSCs *In Vitro* and *In Vivo*

We found that single-layer graphene promoted osteogenic differentiation of hASCs and hBMMSCs. This was corroborated by a series of osteogenic indexes at different time points, including early osteogenic transcription factor Runx2, middle-period osteogenesis-related enzyme ALP, middle-and-late-period osteogenic marker

OCN and late period osteogenesis assay AR-S. Several studies have reported positive results for osteogenic differentiation of MSCs on graphene, multiple-layer graphene, graphene oxide (GO) films and graphene hybrid materials.^{18, 19, 21, 31–33} However, it has been found that different oxidative treatments, particle size, particulate state, oxygen content and the surface charge of GO can significantly impact the biological and toxicological response of cells.^{34–38} Our study demonstrated that single-layer graphene coating is safe and has no negative effects on the

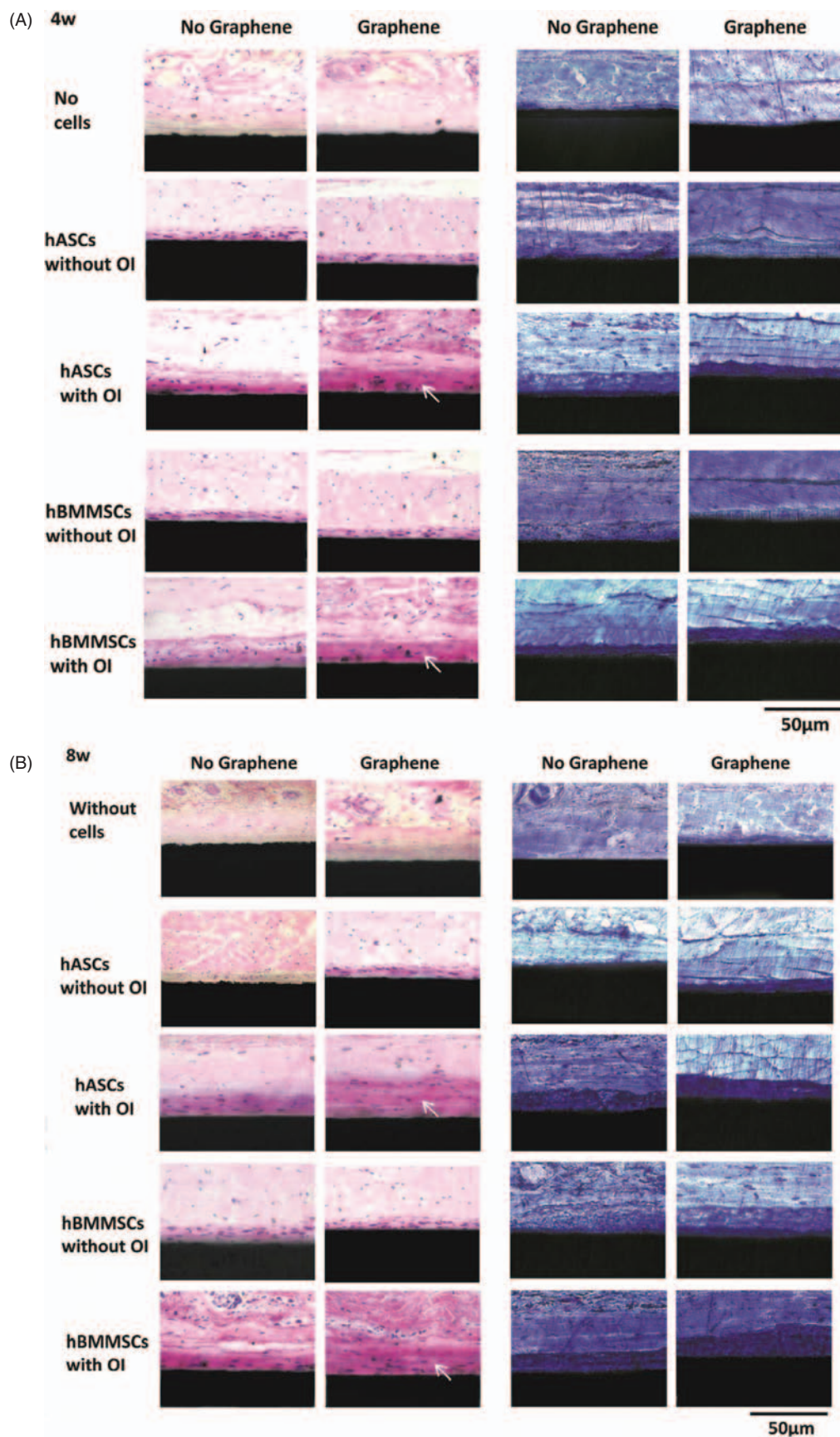


Figure 4. Continued.

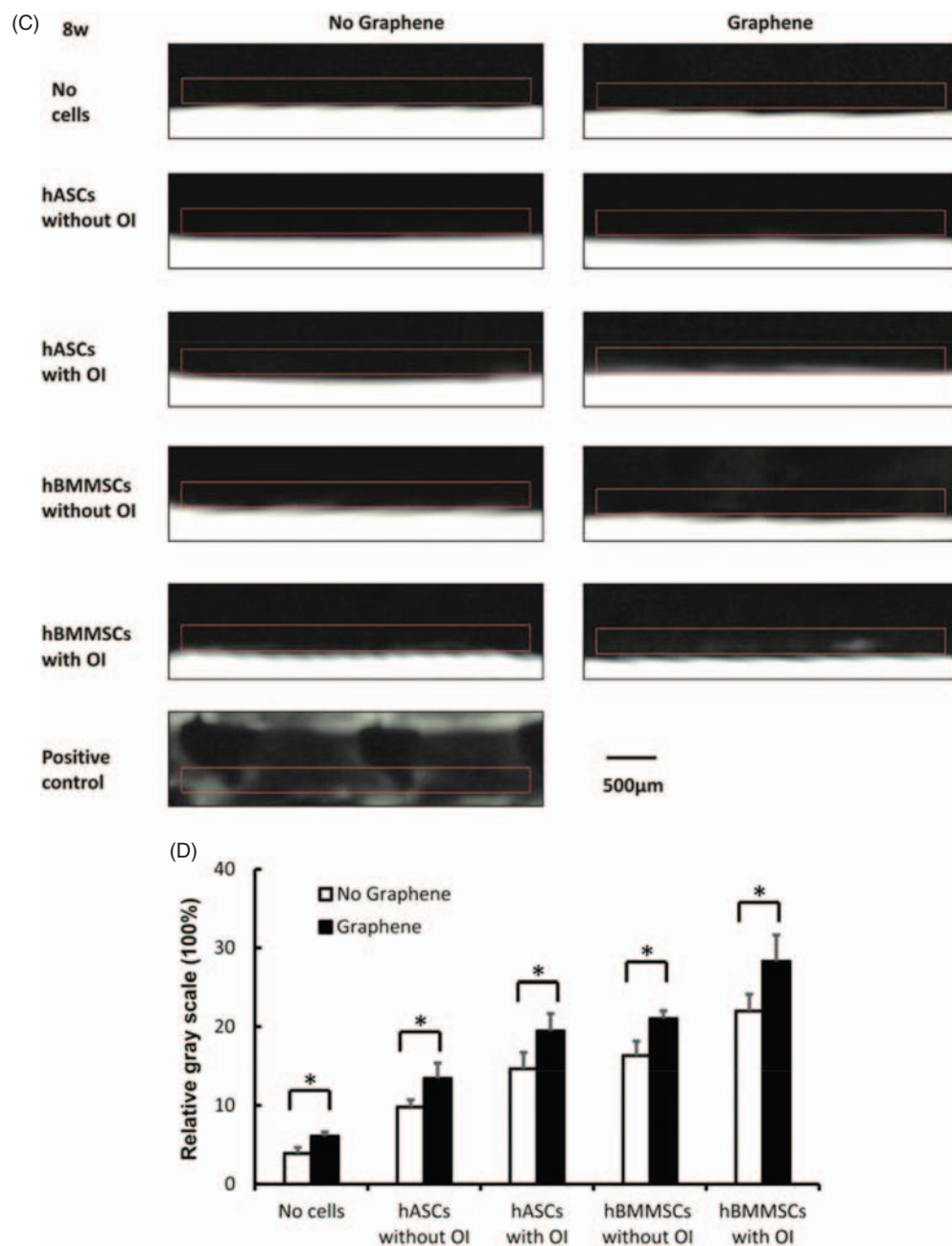


Figure 4. Ectopic bone formation. (A) HE and toluidine blue staining of hard tissue slices after four weeks of implantation at 100 \times magnification. We observed increased amounts of bone matrix formation in the graphene-coated group compared with the graphene-absent group, especially for the hASCs and hBMMSCs osteoinduction (OI) group (white arrows). (B) HE and toluidine blue staining of hard tissue slices after eight weeks of implantation at 100 \times magnification. The neo-bone layer reached a thickness of about 30 μ m in the graphene group with OI for hASCs and hBMMSCs (white arrow). (C) Soft X-ray analyses of ectopic bone formation. Vertebral body slice was detected as positive control and regions of interest (ROI) were drawn (red line box). (D) Relative gray scales of ROI in different groups. * $p < 0.05$.

proliferation of hMSCs. Moreover, single-layer graphene is one-atom thick and can be easily applied to coat scaffolds or substrates with regular surfaces without changing their original shape.¹⁶

To date, the effect of single-layer graphene-coated substrates on the osteogenic differentiation of hMSCs *in vivo* has not been reported. However, there are a few *in vivo*

studies which have suggested that graphene or GO could be used as a reinforcing agent on scaffold materials or drug carriers.^{39–41} In this study, we successfully implanted single-layer graphene-coated Ti disks with hMSCs into the back subcutaneous area of nude mice. Four weeks after implantation, we examined hard tissue slices under a light microscope following HE and toluidine blue staining, with

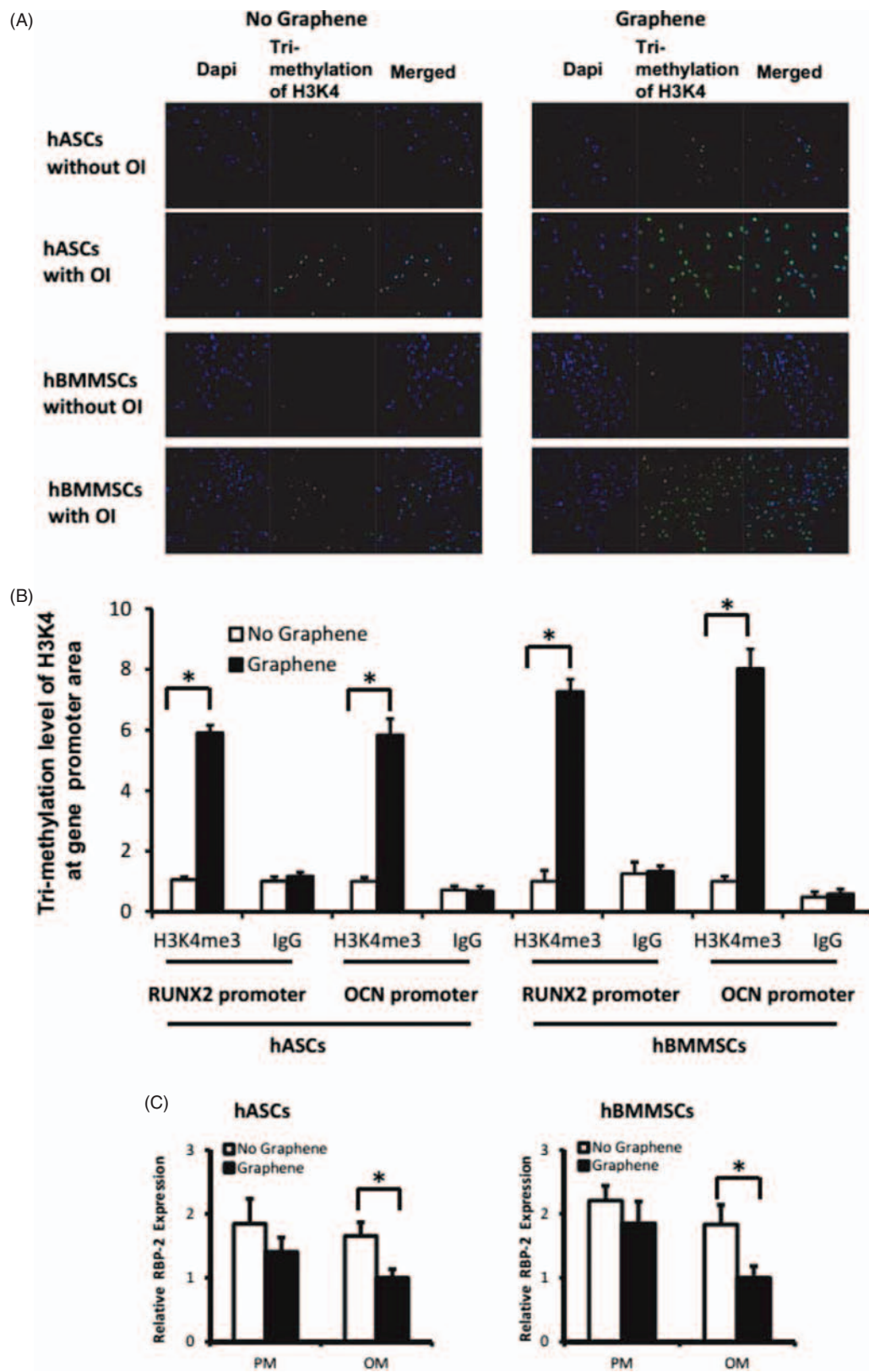


Figure 5. Epigenetic regulation of graphene on hASCs and hBMMSCs. (A) Immunofluorescent staining for tri-methylation of H3K4 in hASCs and hBMMSCs cultured in osteogenic medium for seven days. Tri-methylation of H3K4 is shown in green and nuclei are in blue. (B) ChIP assay of tri-methylation level of H3K4 at the promoter area of osteogenic genes Runx2 and OCN for hASCs and hBMMSCs. (C) Gene expression of demethylase RBP2 at day seven after OI for hASCs and hBMMSCs. * $p < 0.05$. PM: proliferation medium; OM: osteogenic medium.

a larger amount of bone matrix observed in the graphene-coated group compared with the graphene-absent group. Furthermore, we observed more obvious ectopic bone formation in the samples at eight weeks after implantation compared with at four weeks; and again, significantly more bone matrix formation on the surface of graphene-coated group compared with the graphene-absent group. In order to further confirm the bone formation *in vivo*, soft X-ray examination of the hard tissue slices of different groups were performed. We also found that the relative gray scale percentages of all graphene-coated groups were significantly higher than the graphene-absent groups.

These results reveal the osteoinducing ability of single-layer graphene on MSCs both *in vitro* and *in vivo*, and for the first time, put forward the *in vivo* bone regenerative model of graphene. Having established the ectopic bone formation model, our group is now trying to explore the application of graphene-coated dental implants in an orthotopic bone formation model.

Epigenetic Mechanism of Graphene on Osteogenic Differentiation of hASCs and hBMMSCs

It has been demonstrated by us and other researchers that single-layer graphene promotes osteogenic differentiation of MSCs. While, the mechanism by which this proceeds has been explored in terms of morphology,^{17–19} mechanical²⁰ and molecular changes,^{19,21} epigenetic considerations have yet to be explored.^{42–44} We previously discovered that RBP2, a histone demethylase of H3K4, inhibited osteogenic differentiation of hASCs, due to its demethylation activity inhibiting gene expression of osteogenesis-associated genes.^{27,45} Furthermore, we found that RBP2 expression was down-regulated in hASCs in contact with TiO₂ nanotubes.⁴⁶ We therefore asked whether single-layer graphene would also influence the behavior of MSCs through epigenetic regulation?

In this study, we discovered that single-layer graphene could indeed inhibit the expression of RBP2, and therefore, enhance the methylation level of H3K4 at the promoter regions of osteogenesis-associated genes, such as Runx2 and OCN. RBP2 dissociates when stem cells are osteogenetically induced in osteoinductive conditions. Then promoters of osteogenic genes become more accessible and are occupied by activation complexes, including histone methylation; i.e., H3K4 methylation. Hence, the chromatin is altered from a repressed state to an active state, switching on the osteogenic process.²⁷ Here, we performed a ChIP assay to prove that single-layer graphene promoted the osteogenic differentiation of MSCs through inhibition of RBP2 expression.

For the first time, we explored the effect of graphene on cell behavior from the aspect of epigenetic regulation. Aside from H3K4, other histone modification sites, such as methylation and acetylation of H3K9 and H3K27, can also

influence the osteogenic differentiation of stem cells.^{47–50} Therefore it is reasonable to assume that the epigenetic regulation of stem cell lineage is complex, and our study is limited. Epigenetics is central to cellular differentiation and stem cell lineage commitment. A better understanding of the epigenetic mechanism of how geometric cues influence stem cells could improve bone tissue engineering and provide new insights into the modulation of surface modification and stem cell therapy. Therefore, more studies are needed to unveil the epigenetic mechanisms involved and accelerate its clinical translation.

Within the limitation of the present investigation, we believe that single-layer graphene exhibits unique properties and is a promising nano-material in bone tissue engineering. Moreover, the surface topography of single-layer graphene-coated substrates will be persistent. The long lasting effect of graphene on cell differentiation is an important advantage when compared to the short lasting effects of osteoinductive growth factors. However, compared to CVD graphene, the mechanical strength of graphene coatings transferred to distinct substrates cannot be ensured. We speculate that producing graphene directly on the substrate by CVD method may solve this problem. To date, there have been no clinical models reported for the translational application of graphene in medical domains. Our team is currently trying to apply single-layer graphene onto the neck of dental implants as a surface modification material to solve the problem of bone resorption around the implant.

CONCLUSION

We show single-layer graphene accelerates cell adhesion to the substrate without influencing cell proliferation of hMSCs. We also reveal that single-layer graphene promotes osteogenic differentiation of hMSCs *in vitro* and *in vivo* by upregulating methylations level of H3K4 at the promoter regions of osteogenesis-associated genes through inhibiting RBP2 expression. This is the first study to explore the epigenetic mechanism by which single-layer graphene directs stem cell fate.

Acknowledgments: We gratefully acknowledge the support of this work by funding from the National Natural Science Foundation of China (81470769 to Yunsong Liu), the Beijing Natural Science Foundation (7153178 to Yunsong Liu), the Program for New Century Excellent Talents in University from Ministry of Education of China (NCET-11-0026 to Yongsheng Zhou), and the Peking University 985 Program (2012 to Yongsheng Zhou and Chunyang Xiong).

REFERENCES

1. F. R. Rose and R. O. Oreffo, Bone tissue engineering: Hope versus hype. *Biochem. Biophys. Res. Commun.* 292, 1 (2002).
2. M. Dominici, K. Le Blanc, I. Mueller, I. Slaper-Cortenbach, F. Marini, D. Krause, R. Deans, A. Keating, D. Prockop, and

- E. Horwitz, Minimal criteria for defining multipotent mesenchymal stromal cells. The international society for cellular therapy position statement. *Cytotherapy* 8, 315 (2006).
3. E. Nyberg, C. Holmes, T. Witham, and W. L. Grayson, Growth factor-eluting technologies for bone tissue engineering. Drug delivery and translational research. *Drug Deliv. Transl. Res.* (2015), doi: 10.1007/s13346-015-0233-3.
 4. M. M. Martino, P. S. Briquez, K. Maruyama, and J. A. Hubbell, *Adv. Drug Deliv. Rev.* (2015), doi: 10.1016/j.addr.2015.04.007.
 5. K. S. Novoselov, A. K. Geim, S. V. Morozov, D. Jiang, Y. Zhang, S. V. Dubonos, I. V. Grigorieva, and A. A. Firsov, Electric field effect in atomically thin carbon films. *Science* 306, 666 (2004).
 6. C. Lee, X. Wei, J. W. Kysar, and J. Hone, Measurement of the elastic properties and intrinsic strength of monolayer graphene. *Science* 321, 385 (2008).
 7. K. S. Novoselov, V. I. Fal'ko, L. Colombo, P. R. Gellert, M. G. Schwab, and K. Kim, A roadmap for graphene. *Nature* 490, 192 (2012).
 8. M. Yang, J. Yao, and Y. Duan, Graphene and its derivatives for cell biotechnology. *Analyst* 138, 72 (2013).
 9. A. S. Mayorov, R. V. Gorbachev, S. V. Morozov, L. Britnell, R. Jalil, L. A. Ponomarenko, P. Blake, K. S. Novoselov, K. Watanabe, T. Taniguchi, and A. K. Geim, Micrometer-scale ballistic transport in encapsulated graphene at room temperature. *Nano Lett.* 11, 2396 (2011).
 10. A. A. Balandin, Thermal properties of graphene and nanostructured carbon materials. *Nat. Mater.* 10, 569 (2011).
 11. Y. Zhang, L. Zhang, and C. Zhou, Review of chemical vapor deposition of graphene and related applications. *Acc. Chem. Res.* 46, 2329 (2013).
 12. L. Feng and Z. Liu, Graphene in biomedicine: Opportunities and challenges. *Nanomedicine* 6, 317 (2011).
 13. C. Chung, Y. K. Kim, D. Shin, S. R. Ryoo, B. H. Hong, and D. H. Min, Biomedical applications of graphene and graphene oxide. *Acc. Chem. Res.* 46, 2211 (2013).
 14. X. Li, W. Cai, J. An, S. Kim, J. Nah, D. Yang, R. Piner, A. Velamakanni, I. Jung, E. Tutuc, S. K. Banerjee, L. Colombo, and R. S. Ruoff, Large-area synthesis of high-quality and uniform graphene films on copper foils. *Science* 324, 1312 (2009).
 15. S. Bae, H. Kim, Y. Lee, X. Xu, J. S. Park, Y. Zheng, J. Balakrishnan, T. Lei, H. R. Kim, Y. I. Song, Y. J. Kim, K. S. Kim, B. Özyilmaz, J. H. Ahn, B. H. Hong, and S. Iijima, Roll-to-roll production of 30-inch graphene films for transparent electrodes. *Nat. Nanotechnol.* 5, 574 (2010).
 16. A. Reina, X. Jia, J. Ho, D. Nezich, H. Son, V. Bulovic, M. S. Dresselhaus, and J. Kong, Large area, few-layer graphene films on arbitrary substrates by chemical vapor deposition. *Nano Lett.* 9, 30 (2009).
 17. M. Kalbacova, A. Broz, J. Kong, and M. Kalbac, Graphene substrates promote adherence of human osteoblasts and mesenchymal stromal cells. *Carbon* 48, 4323 (2010).
 18. T. R. Nayak, H. Andersen, V. S. Makam, C. Khaw, S. Bae, X. Xu, P. L. Ee, J. H. Ahn, B. H. Hong, G. Pastorin, and B. Özyilmaz, Graphene for controlled and accelerated osteogenic differentiation of human mesenchymal stem cells. *ACS Nano* 5, 4670 (2011).
 19. W. C. Lee, C. H. Lim, H. Shi, L. A. Tang, Y. Wang, C. T. Lim, and K. P. Loh, Origin of enhanced stem cell growth and differentiation on graphene and graphene oxide. *ACS Nano* 5, 7334 (2011).
 20. J. Kim, Y.-R. Kim, Y. Kim, K. T. Lim, H. Seonwoo, S. Park, S.-P. Cho, B. H. Hong, P. H. Choung, T. D. Chung, Y.-H. Choung, and J. H. Chung, Graphene-incorporated chitosan substrata for adhesion and differentiation of human mesenchymal stem cells. *J. Mater. Chem. B* 1, 933 (2013).
 21. D. Depan and R. D. Misra, The interplay between nanostructured carbon-grafted chitosan scaffolds and protein adsorption on the cellular response of osteoblasts: Structure-function property relationship. *Acta Biomater.* 9, 6084 (2013).
 22. M. Gu, Y. Liu, T. Chen, F. Du, X. Zhao, C. Xiong, and Y. Zhou, Is graphene a promising nano-material for promoting surface modification of implants or scaffold materials in bone tissue engineering? *Tissue Eng. Part B Rev.* 20, 477 (2014).
 23. Y. S. Liu, M. E. Ou, H. Liu, M. Gu, L. W. Lv, C. Fan, T. Chen, X. H. Zhao, C. Y. Jin, X. Zhang, Y. Ding, and Y. S. Zhou, The effect of simvastatin on chemotactic capability of SDF-1 α and the promotion of bone regeneration. *Biomaterials* 35, 4489 (2014).
 24. Y. Liu, X. Zhang, Y. Liu, X. Jin, C. Fan, H. Ye, M. Ou, L. Lv, G. Wu, and Y. Zhou, Bi-functionalization of a calcium phosphate-coated Ti surface with slow-release simvastatin and metronidazole to provide antibacterial activities and pro-osteodifferentiation capabilities. *PLoS One* 9, e97741 (2014).
 25. Y. Liu, Y. Zhao, X. Zhang, T. Chen, X. Zhao, G. E. Ma, and Y. Zhou, Flow cytometric cell sorting and *in vitro* pre-osteinduction are not requirements for *in vivo* bone formation by human adipose-derived stromal cells. *PLoS One* 8, e56002 (2013).
 26. Y. Zhou, Y. Ni, Y. Liu, B. Zeng, Y. Xu, and W. Ge, The role of simvastatin in the osteogenesis of injectable tissue-engineered bone based on human adipose-derived stromal cells and platelet-rich plasma. *Biomaterials* 31, 5325 (2010).
 27. W. Ge, L. Shi, Y. Zhou, Y. Liu, G. E. Ma, Y. Jiang, Y. Xu, X. Zhang, and H. Feng, Inhibition of osteogenic differentiation of human adipose-derived stromal cells by retinoblastoma binding protein 2 repression of RUNX2-activated transcription. *Stem Cells* 29, 1112 (2011).
 28. J. Hall, R. G. Sorensen, J. M. Wozney, and U. M. Wikesjö, Bone formation at rhBMP-2-coated titanium implants in the rat ectopic model. *J. Clin. Periodontol.* 34, 444 (2007).
 29. K. S. Brammer, C. J. Frandsen, and S. Jin, TiO₂ nanotubes for bone regeneration. *Trends. Biotechnol.* 30, 315 (2012).
 30. T. Akasaka, A. Yokoyama, M. Matsuoka, T. Hashimoto, and F. Watari, Thin films of single-walled carbon nanotubes promote human osteoblastic cells (Saos-2) proliferation in low serum concentrations. *Mater. Sci. Eng. C—Mater. Biol. Appl.* 30, 391 (2010).
 31. D. Depan, B. Girase, J. S. Shah, and R. D. Misra, Structure-process-property relationship of the polar graphene oxide-mediated cellular response and stimulated growth of osteoblasts on hybrid chitosan network structure nanocomposite scaffolds. *Acta Biomater.* 7, 3432 (2011).
 32. S. Kim, S. H. Ku, S. Y. Lim, J. H. Kim, and C. B. Park, Graphene-biomineral hybrid materials. *Adv. Mater.* 23, 2009 (2011).
 33. J. Kim, K. S. Choi, Y. Kim, K. T. Lim, H. Seonwoo, Y. Park, D. H. Kim, P. H. Choung, C. S. Cho, S. Y. Kim, Y. H. Choung, and J. H. Chung, Bioactive effects of graphene oxide cell culture substratum on structure and function of human adipose-derived stem cells. *J. Biomed. Mater. Res. A* 101, 3520 (2013).
 34. X. Cai, S. Tan, A. Yu, J. Zhang, J. Liu, W. Mai, and Z. Jiang, Sodium 1-naphthalenesulfonate-functionalized reduced graphene oxide stabilizes silver nanoparticles with lower cytotoxicity and long-term antibacterial activity. *Chem. Asian J.* 7, 1664 (2012).
 35. K. H. Liao, Y. S. Lin, C. W. Macosko, and C. L. Haynes, Cytotoxicity of graphene oxide and graphene in human erythrocytes and skin fibroblasts. *ACS Appl. Mater. Interfaces* 3, 2607 (2011).
 36. A. Sasidharan, L. S. Panchakarla, P. Chandran, D. Menon, S. Nair, C. N. Rao, and M. Koyakutty, Differential nano-bio interactions and toxicity effects of pristine versus functionalized graphene. *Nanoscale* 3, 2461 (2011).
 37. B. J. Hong, O. C. Compton, Z. An, I. Eryazici, and S. T. Nguyen, Successful stabilization of graphene oxide in electrolyte solutions: Enhancement of biofunctionalization and cellular uptake. *ACS Nano* 6, 63 (2012).
 38. E. L. Chng and M. Pumera, The toxicity of graphene oxides: Dependence on the oxidative methods used. *Chemistry* 19, 8227 (2013).
 39. W. G. La, M. Jin, S. Park, H. H. Yoon, G. J. Jeong, S. H. Bhang, H. Park, K. Char, and B. S. Kim, Delivery of bone morphogenetic

- protein-2 and substance P using graphene oxide for bone regeneration. *Int. J. Nanomedicine* 1, 107 (2014).
40. C. Gao, T. Liu, C. Shuai, and S. Peng, Enhancement mechanisms of graphene in nano-58S bioactive glass scaffold: Mechanical and biological performance. *Sci. Rep.* 4, 4712 (2014).
 41. W. G. La, S. Park, H. H. Yoon, G. J. Jeong, T. J. Lee, S. H. Bhang, J. Y. Han, K. Char, and B. S. Kim, Delivery of a therapeutic protein for bone regeneration from a substrate coated with graphene oxide. *Small* 9, 4051 (2013).
 42. I. Garcia-Bassets, Y. S. Kwon, F. Telese, G. G. Prefontaine, K. R. Hutt, C. S. Cheng, B. G. Ju, K. A. Ohgi, J. Wang, L. Escoubet-Lozach, D. W. Rose, C. K. Glass, X. D. Fu, and M. G. Rosenfeld, Histone methylation-dependent mechanisms impose ligand dependency for gene activation by nuclear receptors. *Cell* 128, 505 (2007).
 43. L. Ye, Z. Fan, B. Yu, J. Chang, K. Al Hezaimi, X. Zhou, N. H. Park, and C. Y. Wang, Histone demethylases KDM4B and KDM6B promotes osteogenic differentiation of human MSCs. *Cell Stem Cell* 11, 50 (2012).
 44. A. Barkhordarian, J. Sison, R. Cayabyab, N. Mahanian, and F. Chiappelli, Epigenetic regulation of osteogenesis: Human embryonic palatal mesenchymal cells. *Bioinformation* 5, 278 (2011).
 45. R. J. Klose, Q. Yan, Z. Tothova, K. Yamane, H. Erdjument-Bromage, P. Tempst, D. G. Gilliland, Y. Zhang, and W. G. Kaelin, Jr., The retinoblastoma binding protein RBP2 is an H3K4 demethylase. *Cell* 128, 889 (2007).
 46. L. Lv, Y. Liu, P. Zhang, X. Zhang, J. Liu, T. Chen, P. Su, H. Li, and Y. Zhou, The nanoscale geometry of TiO₂ nanotubes influences the osteogenic differentiation of human adipose-derived stem cells by modulating H3K4 trimethylation. *Biomaterials* 39, 193 (2015).
 47. Y. Wei, Y. H. Chen, L. Y. Li, J. Lang, S. P. Yeh, B. Shi, C. C. Yang, J. Y. Yang, C. Y. Lin, C. C. Lai, and M. C. Hung, CDK1-dependent phosphorylation of EZH2 suppresses methylation of H3K27 and promotes osteogenic differentiation of human mesenchymal stem cells. *Nat. Cell Biol.* 13, 87 (2011).
 48. C. M. Teven, X. Liu, N. Hu, N. Tang, S. H. Kim, E. Huang, E. K. Yang, M. Li, J. L. Gao, H. Liu, R. B. Natale, G. Luther, Q. Luo, L. Wang, R. Rames, Y. Bi, J. Luo, H. H. Luu, R. C. Haydon, R. R. Reid, and T. C. He, Epigenetic regulation of mesenchymal stem cells: A focus on osteogenic and adipogenic differentiation. *Stem Cells Int.* 2011, 201371 (2011).
 49. J. Du, Y. Ma, P. Ma, S. Wang, and Z. Fan, Demethylation of epiregulin gene by histone demethylase FBXL11 and BCL6 corepressor inhibits osteo/dentinogenic differentiation. *Stem Cells* 31, 126 (2013).
 50. A. Noer, L. C. Lindeman, and P. Collas, Histone H3 modifications associated with differentiation and long-term culture of mesenchymal adipose stem cells. *Stem Cells Dev.* 18, 725 (2009).